A more sensitive search for $\nu\_\mu \to \nu\_\tau$ oscillations in NOMAD

P. Astier, D. Autiero, A. Baldisseri, M. Baldo-Ceolin, G. Ballocchi, M. Banner, G. Bassompierre, K. Benslama, N. Besson, I. Bird, et al.

▶ **To cite this version:**

P. Astier, D. Autiero, A. Baldisseri, M. Baldo-Ceolin, G. Ballocchi, et al.. A more sensitive search for $\nu\_\mu \to \nu\_\tau$ oscillations in NOMAD. Physics Letters B, 1999, 453, pp.169-186. in2p3-00002525

HAL Id: in2p3-00002525
https://in2p3.hal.science/in2p3-00002525v1

Submitted on 17 May 1999

HAL is a multi-disciplinary open access archive for the deposit and dissemination of scientific research documents, whether they are published or not. The documents may come from teaching and research institutions in France or abroad, or from public or private research centers.

L'archive ouverte pluridisciplinaire **HAL**, est destinée au dépôt et à la diffusion de documents scientifiques de niveau recherche, publiés ou non, émanant des établissements d'enseignement et de recherche français ou étrangers, des laboratoires publics ou privés.

EUROPEAN LABORATORY FOR PARTICLE PHYSICS

CERN-EP/99-32
February 25, 1999

A More Sensitive Search for $\nu_\mu \rightarrow \nu_\tau$ Oscillations in NOMAD

NOMAD Collaboration

P. Astier [n] D. Autiero [h] A. Baldisseri [r] M. Baldo-Ceolin [m]
G. Ballocchi [h] M. Banner [n] G. Bassompierre [a] K. Benslama [i]
N. Besson [r] I. Bird [h,i] B. Blumenfeld [b] F. Bobisut [m] J. Bouchez [r]
S. Boyd [t] A. Bueno [c,x] S. Bunyatov [f] L. Camilleri [h] A. Cardini [j]
P.W. Cattaneo [o] V. Cavasinni [p] A. Cervera-Villanueva [h,v]
G. Collazuol [m] G. Conforto [h,u] C. Conta [o] M. Contalbrigo [m]
R. Cousins [j] D. Daniels [c] H. Degaudenzi [i] T. Del Prete [p]
A. De Santo [h,p] T. Dignan [c] L. Di Lella [h] E. do Couto e Silva [h]
I.J. Donnelly [s,t] J. Dumarchez [n] M. Ellis [t] T. Fazio [a]
G.J. Feldman [c] R. Ferrari [o] D. Ferrère [h] V. Flaminio [p]
M. Fraternali [o] J.-M. Gaillard [a] A. Gandolfo [o] E. Gangler [h,n]
A. Geiser [e,h] D. Geppert [e] D. Gibin [m] S. Gninenko [l] A. Godley [t]
J.-J. Gomez-Cadenas [h,v] J. Gosset [r] C. Gößling [e] M. Gouanère [a]
A. Grant [h] G. Graziani [g] A. Guglielmi [m] C. Hagner [r]
J. Hernando [v] D. Hubbard [c] P. Hurst [c] N. Hyett [k] E. Iacopini [g]
C. Joseph [i] F. Juget [i] M. Kirsanov [l,u] O. Klimov [f] J. Kokkonen [h]
A. Kovzelev [l,o] A. Krasnoperov [a,f] V.E. Kuznetsov [f,h]
S. Lacaprara [m] C. Lachaud [n] B. Lakić [w] A. Lanza [o]
L. La Rotonda [d] M. Laveder [m] A. Letessier-Selvon [n] J.-M. Levy [n]
L. Linssen [h] A. Ljubičić [w] J. Long [b] A. Lupi [g]
E. Manola-Poggioli [a] A. Marchionni [g] F. Martelli [u] X. Méchain [r]
J.-P. Mendiburu [a] J.-P. Meyer [r] M. Mezzetto [m] S.R. Mishra [c]
G.F. Moorhead [k] L. Mossuz [a] P. Nédélec [a] Yu. Nefedov [f]
C. Nguyen-Mau [i] D. Orestano [q] F. Pastore [q] L.S. Peak [t]
E. Pennacchio [u] H. Pessard [a] R. Petti [o] A. Placci [h] A. Pluquet [r]
G. Polesello [o] D. Pollmann [e] B. Popov [f,n] C. Poulsen [k]

To be published in Physics Letters B

P. Rathouit [r] R. Renò [p] G. Renzoni [p] J. Rico [x] P. Riemann [e]
C. Roda [h,p] A. Rubbia [h,x] F. Salvatore [o] K. Schahmaneche [n]
B. Schmidt [e,h] T. Schmidt [e] G. Segneri [p] M. Sevior [k] D. Sillou [a]
F.J.P. Soler [h,t] G. Sozzi [i] D. Steele [b,i] M. Steininger [i] U. Stiegler [h]
M. Stipčević [w] Th. Stolarczyk [r] M. Tareb-Reyes [i] G.N. Taylor [k]
V. Tereshchenko [f] A. Toropin [l] A.-M. Touchard [n] S.N. Tovey [h,k]
M.-T. Tran [i] E. Tsesmelis [h] J. Ulrichs [t] L. Vacavant [i]
M. Valdata-Nappi [d] V. Valuev [f,j] F. Vannucci [n] K.E. Varvell [s,t]
M. Veltri [u] V. Vercesi [o] D. Verkindt [a] J.-M. Vieira [i]
T. Vinogradova [j] M.-K. Vo [r] S. Volkov [l] F.V. Weber [c,h]
T. Weisse [e] F.F. Wilson [h] L.J. Winton [k] B.D. Yabsley [t]
H. Zaccone [r] K. Zuber [e] P. Zuccon [m]

[a] *LAPP, Annecy, France*
[b] *Johns Hopkins Univ., Baltimore, MD, USA*
[c] *Harvard Univ., Cambridge, MA, USA*
[d] *Univ. of Calabria and INFN, Cosenza, Italy*
[e] *Dortmund Univ., Dortmund, Germany*
[f] *JINR, Dubna, Russia*
[g] *Univ. of Florence and INFN, Florence, Italy*
[h] *CERN, Geneva, Switzerland*
[i] *University of Lausanne, Lausanne, Switzerland*
[j] *UCLA, Los Angeles, CA, USA*
[k] *University of Melbourne, Melbourne, Australia*
[l] *Inst. Nucl. Research, INR Moscow, Russia*
[m] *Univ. of Padova and INFN, Padova, Italy*
[n] *LPNHE, Univ. of Paris VI and VII, Paris, France*
[o] *Univ. of Pavia and INFN, Pavia, Italy*
[p] *Univ. of Pisa and INFN, Pisa, Italy*
[q] *Roma Tre University and INFN, Rome, Italy*
[r] *DAPNIA, CEA Saclay, France*
[s] *ANSTO Sydney, Menai, Australia*
[t] *Univ. of Sydney, Sydney, Australia*
[u] *Univ. of Urbino, Urbino, and INFN Florence, Italy*
[v] *IFIC, Valencia, Spain*
[w] *Rudjer Bošković Institute, Zagreb, Croatia*
[x] *ETH Zürich, Zürich, Switzerland*

Abstract

With additional data and improved algorithms, we have enhanced the sensitivity of our appearance search for $\nu_\mu \to \nu_\tau$ oscillations in the NOMAD detector in the CERN-SPS wide-band neutrino beam. The search uses kinematic criteria to identify ν_τ charged current interactions followed by decay of the τ^- to one of several decay modes. Our "blind" analyses of deep-inelastic scattering data taken in 1996 and 1997, combined with consistent reanalyses of previously reported 1995 data, yield no oscillation signal. For the two-family oscillation scenario, we present the contour outlining a 90% C.L. confidence region in the $\sin^2 2\theta_{\mu\tau} - \Delta m^2$ plane. At large Δm^2, the confidence region includes $\sin^2 2\theta_{\mu\tau} < 1.2 \times 10^{-3}$ (a limit 3.5 times more stringent than in our previous publication), while at $\sin^2 2\theta_{\mu\tau} = 1$, the confidence region includes $\Delta m^2 < 1.2$ eV$^2/c^4$.

Key words: neutrino oscillations

1 Introduction

In a recent article [1], we have reported the first results from a search for $\nu_\mu \to \nu_\tau$ oscillations using the NOMAD detector to look for ν_τ appearance in the CERN wide-band neutrino beam from the 450 GeV proton synchrotron (SPS). The detection of an oscillation signal relies on the identification of ν_τ charged-current (CC) interactions using kinematic criteria. The analysis described in Ref. [1] was based on data collected in 1995, corresponding to approximately 162 000 ν_μ CC events in the detector fiducial volume. No oscillation signal was observed.

In this letter we report a new search for $\nu_\mu \to \nu_\tau$ oscillations with increased sensitivity from the analysis of a much larger data sample which includes data collected during the 1995, 1996, and 1997 runs (with a small fraction of 1997 data not yet analyzed) and corresponds to $\sim$ 950 000 ν_μ CC events for the full sample [2]. This analysis is based on deep inelastic interactions and its results are combined with the published results from the analysis of low-multiplicity events in the 1995 data [1]. The algorithms for many phases of the analysis (including drift chamber alignment, track and vertex reconstruction, photon reconstruction in the presence of hadronic deposition in the electromagnetic calorimeter [3], and subdetector matching) have been improved, complementing improvements in the Monte Carlo (MC) event generation and simulation.

2 NOMAD detector and neutrino beam

The NOMAD detector is described in Refs. [1,4]. Inside a 0.4 T magnetic field, it consists of an active target (2.7 tons) of drift chambers (DC) followed by a transition radiation detector (TRD) [5], a preshower detector (PS), and an electromagnetic calorimeter (ECAL) [6]. A hadron calorimeter (HCAL) and two muon stations are located just after the magnet coil.

The neutrino interaction trigger [7] consists of a coincidence between two planes of counters located after the active target, in the absence of a signal from a large area system of veto counters in front of the NOMAD detector.

In the absence of oscillations, the relative beam composition is predicted to be $\nu_\mu : \bar{\nu}_\mu : \nu_e : \bar{\nu}_e = 1.00 : 0.061 : 0.0094 : 0.0024$, with average energies of 23.5, 19.2, 37.1, and 31.3 GeV, respectively [8]. Neutrinos are mostly produced in a 290 m long decay tunnel at an average distance of 625 m from the detector.

3 Event samples

For the data sample corresponding to 950 000 ν_μ CC interactions, we expect 24 000 $\bar{\nu}_\mu$ CC, 14 000 ν_e CC, and 1500 $\bar{\nu}_e$ CC interactions, and approximately 310 000 neutral current (NC) interactions. In order to estimate the background from these ordinary neutrino interactions, we have generated large MC samples, exceeding the size of the data samples by a factor varying between 2 (for ν_μ CC events) and 10 (for $\bar{\nu}_\mu$ CC, ν_e CC, and $\bar{\nu}_e$ CC events). In addition, we have generated $\sim 10^5$ ν_τ CC interactions for each τ^- decay channel. Our simulation program is based on modified versions of LEPTO 6.1 [9] and JETSET 7.4 [10] with Q^2 and W^2 cutoff parameters removed, and with τ mass and polarization effects included. We use the nucleon Fermi motion distribution of Ref. [11], truncated at 1 GeV/c. A full detector simulation based on GEANT [12] is performed.

4 Analysis principles

We search for ν_τ CC interactions by identifying τ^- decays to $e^-\bar{\nu}_e\nu_\tau$, inclusive decays to one or three charged hadron(s) + ν_τ, and exclusive decays to $\rho^-\nu_\tau$, for a total branching fraction of $\sim 82\%$.

Neutrino interactions in the active target are first selected by requiring the presence of at least two tracks consistent with having a common vertex in the

detector fiducial volume [1]. We then apply quality cuts to ensure that events are not seriously affected by reconstruction inefficiencies, and that charged particle momenta and photon energies are precisely measured. These cuts, based on approximate charge balance at the primary vertex and on the estimated momentum and energy errors, typically remove 15% of the events.

The next analysis steps are:

(1) Identification of the particle (or particles) consistent with being produced in τ decay. We denote this visible particle or system of particles (from the candidate τ) by $\tau_{\rm V}$ and its momentum by $\vec{p}^{\tau_{\rm V}}$.
(2) Reconstruction of the associated hadronic system (called H), as outlined in Ref. [1]. Improvements in the details of the algorithm (along with MC improvements) have reduced the data/MC discrepancy in the missing transverse momentum, but we still rely on the Data Simulator (Sec. 4.1) to correct for remaining differences. We denote the total momentum of H by $\vec{p}^{H}$.
(3) Use of kinematic variables to separate the signal from backgrounds.

We search for ν_τ CC interactions with deep-inelastic scattering (DIS) configurations by requiring that p^H be larger than 1.5 GeV/c.

4.1 The Data Simulator

In order to compute reliably background rejections as large as 10^5, the MC results are corrected using a Data Simulator based on the data themselves [1]. We perform this correction by using a sample of *measured* ν_μ CC events in the real data, removing the identified muon, and replacing it with a MC-generated lepton ℓ. If $\ell \equiv \nu$ one obtains fake neutral current events. If $\ell \equiv e^-$, a large statistics sample of fake ν_e CC events is obtained after correcting for the relative ν_e/ν_μ flux and e/μ identification efficiency. Finally, if ℓ is a τ^- followed by a simulation of its decay into the channel under study, a large sample of fake τ signal events is generated. For all these samples, collectively referred to as the Data Simulator (DS), the hadronic system is taken from the data themselves by construction.

The same procedure can be applied to reconstructed ν_μ CC MC events (Monte Carlo Simulator, MCS). A comparison of the result of the MCS to the standard MC yields a powerful check of the validity of the muon replacement procedure and the correction applied. On the other hand, a comparison of the DS to the MCS gives a direct measure of the effect of the difference between the data and the MC, mainly due to the hadronic system. All signal and background efficiencies ϵ are then obtained from the relation $\epsilon = \epsilon_{\rm MC} \times \epsilon_{\rm DS}/\epsilon_{\rm MCS}$ (see Ref. [1]). For events passing all cuts, the factor $\epsilon_{\rm DS}/\epsilon_{\rm MCS}$ is within 18% of

unity for τ decay events, but can be as large as 1.8 for background events.[1] All "MC" numbers and plots in this paper are already corrected by the Data Simulator, if relevant. The quoted errors reflect the statistical uncertainties from both MC and DS samples.

4.2 Blind analysis

The study of events from real data in the region of kinematic variables where a signal is expected may introduce biases in the event selection resulting in incorrect background estimates. In order to avoid this problem we used for each τ^- decay channel a procedure referred to as "blind analysis", which includes the following:

(1) All backgrounds and the signal efficiency, corrected using the Data Simulator, are estimated as a function of the cuts applied to the relevant variables before looking at the data.
(2) Cuts are defined for τ^- candidate event selection using the information from the previous step in order to optimize the sensitivity to oscillations. Here the sensitivity is defined as the average upper limit that would be obtained by an ensemble of experiments with the same expected mean background, in the absence of true signal events [13]. These cuts define the signal region in the space of relevant variables hereafter named the "box".
(3) The analysis is not allowed to look at data events in the box. It must first be demonstrated that the predicted background agrees with the numbers of data events seen outside the box and that these predictions are robust. The analysis was not blind to data from 1995 [1], which constitutes only 20% of the total sample.
(4) A check is made by performing an identical search for $\bar{\nu}_\mu \to \bar{\nu}_\tau$ oscillations, where no τ^+ signal is expected because of the small $\bar{\nu}_\mu$ content (see Sec. 2) in the beam. In this analysis there is no blind box and data can be studied over the entire space of relevant variables. Agreement between data and background predictions must be demonstrated, except possibly in cases where backgrounds such as charm production are known to affect only the τ^+ search.
(5) When more than one independent analysis of the same channel is performed, we select the analysis with the best sensitivity *before* opening its box.

[1] The net correction factors for total background in each DIS analysis are 1.8 for $\tau^- \to e^-\bar{\nu}_e\nu_\tau$, 1.2 for $\tau^- \to h^-(n\pi^0)\nu_\tau$, 1.8 for $\tau^- \to \rho^-\nu_\tau$, and 1.1 for $\tau^- \to \pi^-\pi^+\pi^-(n\pi^0)\nu_\tau$.

Only when these steps have been fulfilled is the analysis allowed to look for a possible τ^- signal inside the box.

4.3 Definition of variables

To separate signal from background, the analysis of each τ decay mode makes use of kinematic variables selected from the following list:

- $E_{\rm vis}$, the total visible energy of the event.
- $\vec{p}_T^{\,\tau_{\rm V}}$ and $\vec{p}_T^{\,H}$, the transverse momenta of the *visible* tau decay product(s) and of the associated hadronic system, respectively.
- $\vec{p}_T^{\,m}$, defined as $-(\vec{p}_T^{\,\tau_{\rm V}} + \vec{p}_T^{\,H})$ and interpreted as a measurement of the "missing" transverse momentum due to the neutrino(s) from τ decay.
- M_T, the transverse mass (assuming massless decay products) given by $M_T^2 = 4p_T^{\tau_{\rm V}} p_T^m \sin^2(\phi_{\tau_{\rm V} m}/2)$, where $\phi_{\tau_{\rm V} m}$ is the angle between $\vec{p}_T^{\,\tau_{\rm V}}$ and $\vec{p}_T^{\,m}$. For true τ events, $M_T \leq m_\tau$, up to detector resolution and Fermi motion effects.
- Q_T, the component of $\vec{p}^{\,\tau_{\rm V}}$ perpendicular to the total visible momentum vector (including $\tau_{\rm V}$). Large Q_T implies that $\tau_{\rm V}$ is well isolated from the remaining hadronic jet.
- $Q_{\rm Lep}$, the component of $\vec{p}^{\,\tau_{\rm V}}$ perpendicular to $\vec{p}^{\,H}$. Its function is very similar to Q_T, but it is more useful when p^H is small.
- $\phi_{\tau_{\rm V} H}$, ϕ_{mH}, the angles in the transverse plane between $\vec{p}_T^{\,H}$ and the visible and invisible decay products, respectively [14].
- Ratios of linear combinations of p_T^m, $p_T^{\tau_{\rm V}}$, and p_T^H, equivalent to functions of $\phi_{\tau_{\rm V} H}$ and ϕ_{mH}.
- $\theta_{\nu p}$, the angle between the neutrino beam direction and the total visible momentum vector of the event.
- $\theta_{\nu H}$, the angle between the neutrino beam direction and the hadronic jet.
- $\theta_{\rm iso}$, the isolation angle, defined as the minimum angle between a τ decay product and any other track in the event.

For most channels, combinations of these and other variables are used to build a likelihood ratio (denoted by λ). The likelihood functions (denoted by $\mathcal{L}$) entering this ratio are approximated by the product of one, two, or three dimensional (1D, 2D, 3D) probability density functions of these variables. As is common practice, we use the logarithm of this ratio, $\ln\lambda$.

The subset of variables used for each decay channel is given in the following sections, which describe the analyses performed for the four τ^- decay channels mentioned in Sec. 4.

5 $\tau^- \to e^-\bar{\nu}_e\nu_\tau$ decays

Following the general principles of Sec. 4, the search for $\tau^- \to e^-\bar{\nu}_e\nu_\tau$ proceeds by: identifying a prompt electron in an event with no other prompt leptons; reconstructing the hadronic system; and separating $\tau^- \to e^-\bar{\nu}_e\nu_\tau$ from backgrounds using likelihood ratios based on kinematic variables. The effect of the cuts is shown in Table 1, which also gives the results when a positron is chosen. The positron data also contains a significant component from charm production and decay in ν_μ CC interactions.

5.1 Prompt electron identification

In the electron identification step, we consider DC tracks with $p > 1.5$ GeV/c which are associated to the primary vertex, and we apply requirements to reject hadrons based on: TRD identification algorithms [5]; the PS pulse height [6]; the ECAL cluster shape [3]; and consistency of the associated electromagnetic (EM) energy and DC momentum of the candidate. The magnitude of the electron momentum vector is given by our best estimate of the electron initial energy obtained by adding up all the EM energy clusters in a "bremsstrahlung strip" in the bending plane, also adding in positron or electron tracks from bremsstrahlung photons which convert in the DC. We require that this energy, $E_{\rm e}^{\rm tot}$, be consistent with the fitted momentum at the first hit of the track. The direction of the electron momentum is the initial direction of its DC track.

Overall, these requirements achieve a charged pion rejection factor of 10^4. Secondary electrons from Dalitz decays and from photons converting close to the primary vertex are suppressed by requiring that the candidate electron does not form an invariant mass of less than 50 MeV/c^2 with any particle of opposite charge. After these cuts only one out of 1500 π^0's yields an electron which is misidentified as being of primary origin.

These requirements yield an efficiency of 18.6% for prompt electrons from $\tau^- \to e^-\bar{\nu}_e\nu_\tau$, while accepting only 4.7×10^{-5} of ν_μ CC and 3.9×10^{-4} of neutral currents (line 1 of Table 1).

5.2 Kinematic selection of $\tau^- \to e^-\bar{\nu}_e\nu_\tau$

The selected events are mostly ν_e CC interactions, with a genuine primary electron, and ν_μ NC events, with an electron from photon conversion or π^0 Dalitz decay. In ν_e CC events, the electron is typically well-isolated and balances the transverse momentum of the hadron jet. In ν_μ NC events, the electron is

typically embedded in the hadron jet, with transverse momentum somewhat aligned with it. Signal $\tau^- \to e^- \bar{\nu}_e \nu_\tau$ events tend to lie between these two extremes: the neutrinos carry away transverse momentum so that the electron transverse momentum is somewhat less than, and not exactly opposite to, that of the hadron jet. Furthermore, $\tau^- \to e^- \bar{\nu}_e \nu_\tau$ events would typically be less energetic than ν_e CC events, not only because of the unobserved neutrinos, but also because the ν_μ's in the beam are on average less energetic than the ν_e's (see Sec. 2). Finally, as noted above, the transverse mass M_T of signal events is typically at or below the τ mass.

To classify events using these kinematic differences, we construct two approximate likelihood functions. The first, $\mathcal{L}_{e1}$, is designed to distinguish $\tau^- \to e^- \bar{\nu}_e \nu_\tau$ signal events from ν_μ NC background. It is formed from 2D and 3D distributions (thereby including correlations) of combinations of $\theta_{\nu p}$, $\theta_{\nu H}$, $\theta_{\rm iso}$, Q_T, $E_{\rm e}^{\rm tot}$, and M_T. For each event, we then define the likelihood ratio $\ln \lambda_{e1}$ to be the ratio of the likelihood $\mathcal{L}_{e1}$ constructed from signal events and the likelihood $\mathcal{L}_{e1}$ constructed from ν_μ NC events. High values of this ratio effectively select electrons isolated from the hadronic jets.

The second function, $\mathcal{L}_{e2}$, is designed to distinguish $\tau^- \to e^- \bar{\nu}_e \nu_\tau$ signal events from ν_e CC background. It is formed from the product of two 3D distributions: ($p_T^{\tau \rm V}$, p_T^H, $\phi_{\tau \rm V H}$) and ($E_{\rm vis}$, $\theta_{\nu p}$, $Q_{\rm Lep}$). This factorization approximates the true likelihood function and includes many of the important correlations among the variables. For each event, we then define the likelihood ratio $\ln \lambda_{e2}$ to be the ratio of the likelihood $\mathcal{L}_{e2}$ constructed from signal events and the likelihood $\mathcal{L}_{e2}$ constructed from ν_e CC events.

Before constructing these likelihood functions, we require that $\phi_{\tau \rm V H} + \phi_{mH} < 1.96\pi$ and that $p_T^{\tau \rm V} > 0.1$ GeV/c. These cuts ensure that the transverse angles are well defined (line 2 of Table 1).

Figure 1 contains scatter plots among variables used to construct $\mathcal{L}_{e1}$ and $\mathcal{L}_{e2}$, illustrating differences between signal and backgrounds. The combined rejection power of the two likelihood ratios can be seen in Fig. 2, which is a scatter plot of $\ln \lambda_{e2}$ vs $\ln \lambda_{e1}$, for MC simulations of signal and backgrounds. The large boxed region (the blind box) at large values of both ratios contains little background but is populated by signal events. It is subdivided into five "sub-boxes" which have varying signal-to-background ratios. After we chose these subdivisions and subsequently opened the box, we found that the data (Fig. 2(d)) populated it in a manner consistent with background expectations, for both the total number of events (5 seen vs 6.3 expected) and the distribution within the sub-boxes (see Tables 1 and 2). Figure 3 shows the distribution of $\ln \lambda_{e2}$, for events passing all cuts except the one on $\ln \lambda_{e2}$, for the sum of simulated backgrounds (normalized to the data sample sizes of Sec. 3), the $\tau^- \to e^- \bar{\nu}_e \nu_\tau$ simulation (arbitrarily normalized), and the data, in

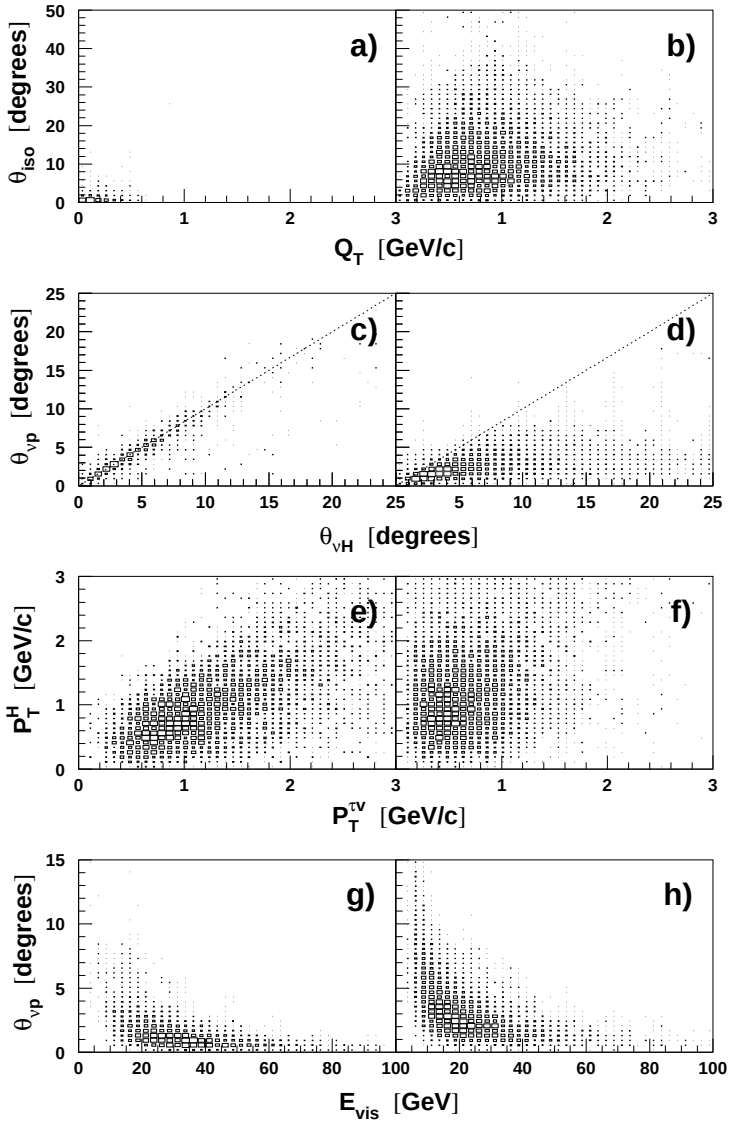

Fig. 1. Scatter plots for some pairs of variables used to construct $\mathcal{L}_{e1}$ and $\mathcal{L}_{e2}$, for MC events of type ν_μ NC ((a) and (c)), ν_e CC ((e) and (g)), and $\tau^- \to e^- \bar{\nu}_e \nu_\tau$ (four plots on the right).

good agreement with background expectations.

6 Inclusive one-prong hadronic decays

The search for $\tau^- \to h^-(n\pi^0)\nu_\tau$ decays, where h^- is a hadron and $n \geq 0$, proceeds in three steps: the selection of the h^- candidate; the rejection of ν_μ, $\bar{\nu}_\mu$, ν_e, and $\bar{\nu}_e$ CC interactions; and the final separation of the signal from the

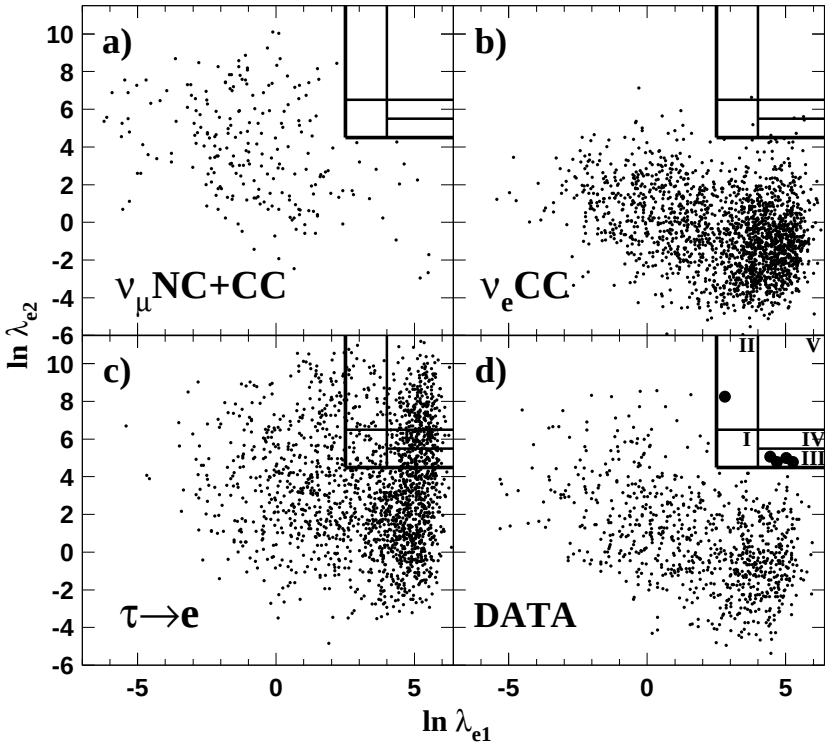

Fig. 2. Scatter plot of $\ln\lambda_{e2}$ vs $\ln\lambda_{e1}$ for (a) MC ν_μ NC (and the few surviving ν_μ CC), (b) MC ν_e CC, (c) MC $\tau^- \to e^-\bar{\nu}_e\nu_\tau$, and (d) data (the large full circles represent the five surviving events in the box). The large box at the upper right corner indicates the signal region and is divided into sub-boxes.

Table 1
The effect of $\tau^- \to e^-\bar{\nu}_e\nu_\tau$ selection cuts on simulated signal events, on background ν_e CC, ν_μ CC and NC events, and on the data. The ν_τ CC column shows the $\tau^- \to e^-\bar{\nu}_e\nu_\tau$ efficiency. In the ν_μ CC and NC columns, small contributions from $\bar{\nu}$ are included. The backgrounds are normalized to the data sample sizes of Sec. 3. The sum of all 3 backgrounds is also shown, as is the effect of the cuts on the positron control sample.

Sample	ν_τCC	ν_e CC	$\bar{\nu}_e$ CC	ν_μ CC		NC		Bkgnd Sum		Data	
Charge	–	–	+	–	+	–	+	–	+	–	+
$e^\pm$ ID	0.186	1139	155	43	140	118	118	1300	413	1232	442
$p_T^{\tau\mathrm{V}} > 0.1$ GeV/c	0.150	981	113	27	105	68	72	1076	290	957	299
$\ln\lambda_{e1} > 2.5$	0.093	477.3	57.5	9.9	27.0	4.0	6.4	491.2	90.9	456	82
$\ln\lambda_{e2} > 4.5$	0.035	6.3 ± 1.0	1.0 ± 0.4	$0.0^{+0.9}_{-0.0}$	4.0 ± 1.5	$0.0^{+0.8}_{-0.0}$	2.4 ± 1.4	$6.3^{+1.6}_{-1.0}$	7.4 ± 3.1	5	7

background by means of kinematic criteria.

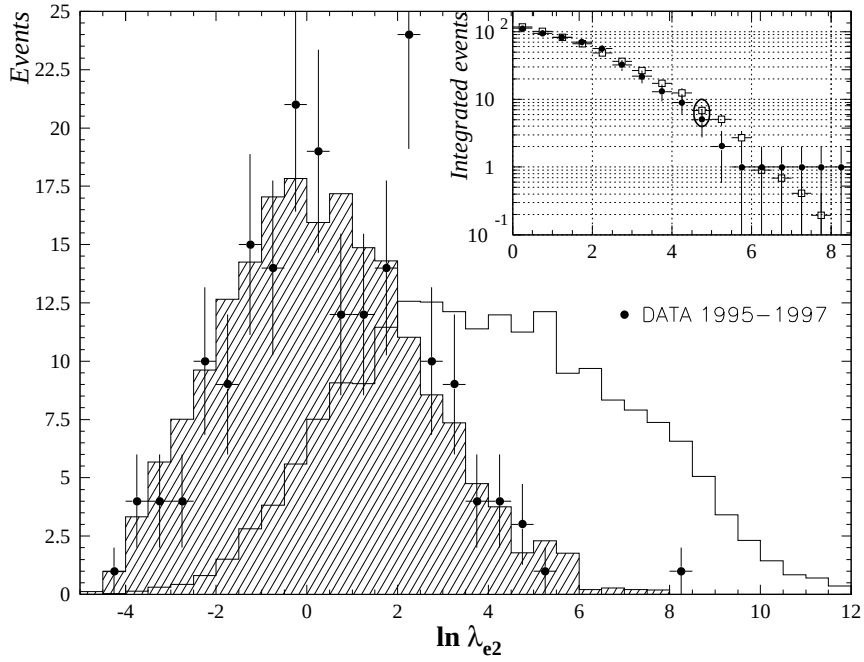

Fig. 3. Histogram of $\ln \lambda_{e2}$ for events passing all cuts except the one on $\ln \lambda_{e2}$, for sum of simulated backgrounds (shaded), $\tau^- \to e^- \bar{\nu}_e \nu_\tau$ simulation (unshaded), and data (points with statistical error bars). The inset gives, for each value of $\ln \lambda_{e2}$, the total number of events beyond that value, for data (dots) and expected background (squares); the encircled points are at the boundary of the signal region.

Table 2
Number of events (total background and data) in each of the sub-boxes of the $\tau^- \to e^- \bar{\nu}_e \nu_\tau$ signal region (see Fig. 2). $N_\tau^{\max}$ is described in Sec. 9; it is the number of $\tau^- \to e^- \bar{\nu}_e \nu_\tau$ events expected in that sub-box if the $\nu_\mu \to \nu_\tau$ oscillation probability were unity.

Sub-box #	Total background	Data	$N_\tau^{\max}$
I	1.19 ± 0.39	0	212
II	0.42 ± 0.27	1	258
III	3.01 ± 0.67	4	620
IV	1.45 ± 0.50	0	535
V	0.28 ± 0.24	0	1193

6.1 Selection of the h^- candidate

In this step we take the highest-p_T negatively-charged primary track to be the h^- candidate. We then require that it be one of the two highest-p_T tracks (of either charge) in the event, that its momentum $p^{\tau\nu}$ be between 3 and 150 GeV/c, that it be associated with an energy deposition in ECAL, and that it not be identified as a muon or an electron.

In the control search for $\bar{\nu}_\mu \to \bar{\nu}_\tau$ oscillations we apply the same criteria to the highest-p_T positively-charged primary track.

6.2 Rejection of background from CC interactions

In order to remove backgrounds from CC ν_μ, $\bar{\nu}_\mu$, ν_e or $\bar{\nu}_e$ interactions, we first apply the following requirements to the $h^\pm$ candidate track:

- no associated muon chamber hits;
- energy deposition in the ECAL or HCAL inconsistent with that of a minimum ionizing particle;
- energy deposition in the TRD, PS or ECAL inconsistent with that of an electron.

These requirements remove background events in which the $h^\pm$ candidate is a misidentified lepton. In addition, we apply a general lepton veto by rejecting events with the following properties:

- presence of a reconstructed track segment in the muon detectors;
- presence of a high p_T track that could have escaped muon or electron identification;
- presence of a primary, high p_T electron candidate, as identified by much looser criteria than those used in Sec. 5.

At this stage of the analysis we apply a kinematic preselection by requiring $M_T < 4$ GeV/c^2 and $p_T^H > 1.3$ GeV/c. After these requirements there is still residual background from ν_μ CC interactions in which the outgoing μ^- is selected as the h^- because it either decayed in flight or suffered a highly inelastic interaction in the calorimeters and failed to reach the muon detectors. This irreducible muon veto inefficiency was measured by studying a large sample of muons originating from a near-by test beam and crossing the NOMAD detector outside the neutrino spills. It varied between $(4.0 \pm 0.3) \times 10^{-4}$ at muon momenta below 10 GeV/c and $(0.3 \pm 0.1) \times 10^{-4}$ above 20 GeV/c. This background is reduced by exploiting the different momentum distributions and kinematic configurations of ν_μ CC events and signal. We build a likelihood

Table 3
The effect of $\tau^- \to h^-(n\pi^0)\nu_\tau$ selection cuts on simulated signal events, on various background samples, and on the data. The ν_τ CC column shows the $\tau^- \to h^-(n\pi^0)\nu_\tau$ efficiency. The effect of the cuts on the positive control sample is also shown.

Sample	ν_τ CC	ν_μ CC		$\bar{\nu}_\mu$ CC		ν_μ NC		ν_e CC		$\bar{\nu}_e$ CC		Data	
Charge	–	–	+	–	+	–	+	–	+	–	+	–	+
$h^\pm$ candidate	0.40	13626	20579	206	92	43076	33912	3052	1488	163	337	64486	55129
Lepton veto	0.14	2649	5648	71	26	22959	19411	59	110	14	5	19616	18136
Presel., $\ln\lambda_{h\mu} > -4$	0.045	111	176	4.0	2.1	3994	2953	8.8	16	3	1.0	4185	3227

based on 3D distributions of the variables Q_T, $\rho_H = p_T^H/(p_T^m + p_T^H + p_T^{\tau_V})$ and $\rho_{\tau_V} = p_T^{\tau_V}/(p_T^m + p_T^H + p_T^{\tau_V})$ using samples of simulated $\tau^- \to h^-(n\pi^0)\nu_\tau$ events and ν_μ CC events from real data. The logarithm of the ratio between signal and background likelihoods, $\ln\lambda_{h\mu}$, is shown in Fig. 4(a). The requirement $\ln\lambda_{h\mu} > -4$ rejects 50% of the ν_μ CC background while keeping 80% of the signal.

The signal, background, and data reduction from all selection criteria described so far is given in Table 3 for both h^- and h^+ candidates.

6.3 Final background rejection and signal selection

In the third step we use kinematic criteria to reject residual backgrounds (mainly from NC interactions). Five variables, Q_T, M_T, p_T^H, $\rho_m = p_T^m/(p_T^m + p_T^{\tau_V} + p_T^H)$, and $y_{\rm Bj} = p^H/(p^{\tau_V} + p^H)$ enter into the construction of approximate multidimensional likelihood functions for signal and backgrounds. Each likelihood function is itself the product of a 3D likelihood depending on Q_T, M_T and ρ_m with two likelihoods which depend on p_T^H and $y_{\rm Bj}$, respectively. The distribution of the logarithm of the ratio between signal and background likelihoods, $\ln\lambda_{h\rm kin}$, is shown in Fig. 4(b) for backgrounds and signal separately. Distributions of Q_T and ρ_m are shown in Figs. 4(c) and 4(d), respectively (these two variables provide the highest rejection power against NC background).

Figure 4(e) shows the number of h^- events above a given $\ln\lambda_{h\rm kin}$ value for the predicted background normalized to the total number of ν_μ CC interactions in the data, and the number of events in the data. The signal box is defined as $\ln\lambda_{h\rm kin} > 7$.

The corresponding distributions for h^+ events are shown in Fig. 4(f). It can be seen from Figs. 4(e) and 4(f) that the data agree with the predicted background outside the signal box for h^-, and everywhere for h^+. The number of $h^\pm$ events found in the box is shown in Table 4, together with the background contributions and with the signal efficiency. The latter has been increased by

Table 4
Signal selection efficiency, background prediction, and numbers of observed events, for $h^{\pm}$ events in the signal box. The ν_τ CC column shows the efficiency for the inclusive one-prong hadronic decay of the τ^- which has a total branching ratio of 49.8%. In the ν_μ CC column, a small contribution from $\bar{\nu}_\mu$ is included. The backgrounds are normalized to the sample sizes of Sec. 3.

$\ln\lambda_{h\mathrm{kin}}$	ν_τ CC	ν_μ CC		ν_μ NC		ν_e CC		$\bar{\nu}_e$ CC		Bkgnd Sum		Data	
Charge	–	–	+	–	+	–	+	–	+	–	+	–	+
> 7	0.0078	2.4	4.9	1.6	2.2	0.7	2.7	0.3	0.1	5.0 ± 1.2	9.9 ± 2.3	5	14
> 8	0.0064	1.4	3.4	1.4	0	0.6	2.2	0.3	0.1	3.7 ± 1.2	5.8 ± 1.4	4	8
> 9	0.0052	1.4	3.0	0.3	0	0.4	2.0	0.2	0.1	2.3 ± 0.8	5.1 ± 1.3	2	6
> 10	0.0048	1.3	3.0	0	0	0.4	1.9	0.2	0.1	1.8 ± 0.7	4.9 ± 1.3	0	6
> 11	0.0044	1.3	2.0	0	0	0.4	1.9	0.2	0.1	1.8 ± 0.7	3.9 ± 1.0	0	5

8% to take into account the efficiency of this analysis to the $\tau^- \to \pi^-\pi^+\pi^-\nu_\tau$ decay channel. The overlap between these events and those selected by the analysis described in Sec. 8 is negligible.

As done in Sec. 5 for the $\tau^- \to e^-$ channel, before opening the signal box we divided it into sub-boxes, so that a more powerful statistical analysis could be performed. We choose the $\ln\lambda_{h\mathrm{kin}}$ intervals 7–9, 9–11 and >11. The numbers of expected background and observed events in these intervals (which we denote as sub-boxes I, II, and III) are listed in Table 7.

7 Exclusive $\tau^- \to \rho^-\nu_\tau$ decays

The search for the exclusive decay $\tau^- \to \rho^-\nu_\tau$ proceeds through the same three steps: the selection of the ρ^- candidate by reconstructing its decay into $\pi^-\pi^0$; rejection of the background from CC interactions; final background rejection and signal selection by kinematic criteria.

As usual, we also perform a search for $\bar{\nu}_\mu \to \bar{\nu}_\tau$ oscillations by applying the same procedure to events with a selected ρ^+ candidate.

7.1 Selection of the $\rho^{\pm}$ candidate

We search for the $\pi^{\pm}$ candidate from the decay chain $\tau^{\pm} \to \rho^{\pm}\nu_\tau \to \pi^{\pm}\pi^0\nu_\tau$ among all primary charged particles with a momentum $p_\pi > 2.5$ GeV/c and inconsistent with being an electron or a muon. We look for photons with energy greater than 0.2 GeV among all photon-like neutral energy clusters in the ECAL or reconstructed photon conversions in the DC. The mass of the pion-photon pair, $M_{\pi\gamma}$, is required to be less than 1 GeV/c^2. If more than one

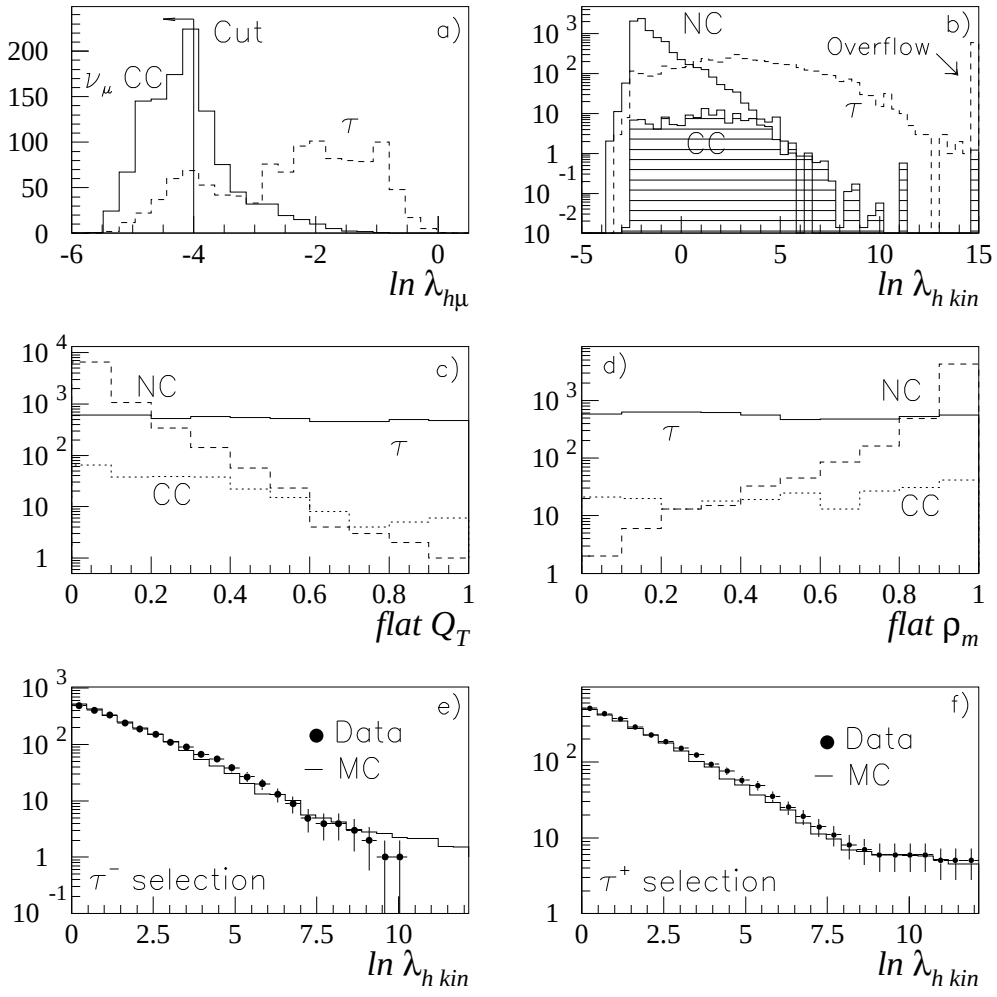

Fig. 4. Distributions from the search for $\tau^- \to h^-(n\pi^0)\nu_\tau$: (a) $\ln\lambda_{h\mu}$ for ν_μ CC background and for signal; (b) $\ln\lambda_{h\mathrm{kin}}$; (c) Q_T, after transformation to the metric in which the signal density is uniform from 0 to 1; (d) ρ_m, after transformation to the metric in which the signal density is uniform from 0 to 1; (e) the integrated number of h^- events above a given $\ln\lambda_{h\mathrm{kin}}$ value for the predicted background and for the data; and (f) the corresponding plot for the τ^+ control search. The uncertainty on the background predictions in (e) and (f) is similar to that of the data points.

$\pi^\pm\gamma$ pair is found, we select the most isolated one, defined to be the one which minimizes the average p_T^2 of the remaining hadronic system with respect to its own axis.

If a $\pi^\pm\gamma$ pair is found, we search for additional photons such that the two-photon invariant mass, $M_{\gamma\gamma}$, is consistent with the π^0 mass ($80 < M_{\gamma\gamma} < 170$ MeV/c^2). If more than one additional photon is found, we choose the

Table 5
The effect of $\tau^- \to \rho^- \nu_\tau$ selection cuts on simulated signal events, on background ν_μ CC, $\bar{\nu}_\mu$ CC, ν_μ NC and ν_e CC events, and on the data. The ν_τ CC column shows the $\tau^- \to \rho^- \nu_\tau$ efficiency. The backgrounds are normalized to the data sample sizes of Sec. 3. The sum of all 4 backgrounds is also shown, as is the effect of the cuts on the positive control sample.

Sample	ν_τ CC	ν_μ CC		$\bar{\nu}_\mu$ CC		ν_μ NC		ν_e CC		Bkgnd Sum		Data	
Charge	–	–	+	–	+	–	+	–	+	–	+	–	+
LC_6	0.057	90.7	31.4	11.6	1.7	195.2	295.5	11.4	19.8	308.9 ± 20.5	348.4 ± 26.8	309	376
LC_5	0.043	51.3	20.2	7.5	1.5	75.5	114.2	9.7	16.4	144.0 ± 10.2	152.3 ± 11.3	144	180
LC_4	0.036	16.6	16.8	2.7	0.7	39.6	60.0	8.3	15.2	67.2 ± 5.7	92.7 ± 6.7	65	111
LC_3	0.020	2.4	6.2	0.7	0.2	7.6	11.5	2.5	7.6	13.2 ± 2.0	25.5 ± 2.2	12	35
LC_2	0.017	1.6	4.4	0.5	0.2	5.2	7.9	2.0	5.6	$9.3^{+2.1}_{-1.5}$	18.1 ± 1.7	7	23
LC_1	0.015	0.8	2.5	0.5	0.2	3.2	4.9	1.0	4.1	$5.5^{+1.6}_{-1.0}$	11.7 ± 1.3	6	14
SBC	0.014	0.8	2.2	0.5	0	2.8	4.3	0.9	3.7	$5.0^{+1.7}_{-0.9}$	$10.2^{+1.4}_{-1.1}$	5	13

one giving the three-body mass, $M_{\pi\gamma\gamma}$, closest to the nominal ρ mass. If no second photon is found and the first photon candidate is consistent with two unresolved photons from π^0 decay, we redefine the first photon candidate to be a π^0. The algorithm selects the correct ρ in 66% of the selected $\tau \to \rho$ events.

7.2 Rejection of background from CC interactions

The criteria used in this step are similar to those used to reject the background from ν_μ, $\bar{\nu}_\mu$, ν_e, and $\bar{\nu}_e$ CC interactions when searching for $\nu_\mu \to \nu_\tau$ oscillations in the inclusive one-prong hadronic decay channel of the τ (see Sec. 6.2). The contribution from $\bar{\nu}_e$ CC interactions is found to be negligible and is ignored in the next step of the analysis.

7.3 Final background rejection and signal selection

To define the signal region, we optimized a set of "signal box cuts" (SBC) on kinematic variables ($E_{\rm vis}$, p_T^H, $p^{\tau\nu}$, M_T, Q_T, $Q_{\rm Lep}$, ϕ_{mH}, $\phi_{\tau_\nu H}$) as well as on the $\pi^\pm$ momentum $p_{\pi^\pm}$, the π^0 momentum p_{π^0}, and $M_{\pi\pi^0}$. An automated cut-tuning procedure was applied to independent MC samples in order to define the cut values which give optimal sensitivity. Using the same variables, we define six sets of looser cuts, LC_1 through LC_6, such that LC_i is tighter than LC_{i+1}. We checked the effect of these cuts on ρ^- events outside the blind box.

Table 5 gives the estimated numbers of background events for ρ^- and ρ^+. Also shown are the numbers of events found in the data. These numbers agree with

the total predicted backgrounds for both ρ^- and ρ^+. In accordance with the blind analysis procedure the signal box for ρ^- events in the data was opened as the very last step of the analysis. No sub-boxes are used in this case since there is no significant variation of the signal-to-background ratio within the box (see Table 7).

The $\tau^- \to \rho^-\nu_\tau$ efficiency is 1.4%. The efficiency of this analysis to other one-prong hadronic decays of the τ^- is 0.4%. Among the decays satisfying all the SBC, 8.4% are also selected by the analysis described in Sec. 6. These events are counted only once when combining the various τ^- decay channels (Sec. 9). All these effects are combined into an effective efficiency of 1.6%, as listed in Table 8.

8 Inclusive three-prong decays of the τ^-

The search for inclusive three-prong decays of the τ^- is optimized for the decay $\tau^- \to \pi^-\pi^+\pi^-\nu_\tau$, but we obtain an appreciable efficiency for other three-prong decays. Hence, all efficiencies for this mode are given with respect to the sum of the relevant modes, which have a total branching ratio of 15.2%.

The $\tau^- \to \pi^-\pi^+\pi^-\nu_\tau$ decay is dominated by the decay chain $\tau^- \to a_1^-(1260)\,\nu_\tau$ $\to \rho^0(770)\,\pi^-\nu_\tau \to \pi^-\pi^+\pi^-\nu_\tau$. Therefore, while the search proceeds similarly to the search for $\tau^- \to h^-(n\pi^0)\nu_\tau$, there are important differences: 1) the internal structure of the 3π system provides additional discriminating power; 2) the three pions have on average lower momentum than the single pion in $\tau^- \to \pi^-\nu_\tau$, so it is less likely that there is muon-chamber evidence that the "pions" are not muons; and 3) due to the high a_1 mass, the ν_τ is on average much less energetic, so missing transverse momentum is less of a signature.

After quality cuts, we reject events with muons identified by the muon stations, or with fewer than four tracks associated with the primary vertex. Thus the hadronic jet contains at least one track, after attribution of three hadrons to the τ decay.

We first choose all three-hadron combinations to be considered as the τ secondaries ($\tau_{\rm V}$, with momentum $\vec{p}^{\,\tau_{\rm V}}$) by requiring that $M_{3\pi} < 1.6$ GeV/c^2, where $M_{3\pi}$ is the invariant mass of the 3π system. We then choose the combination with the highest value of a likelihood ratio constructed to select the decay chain mentioned above. This likelihood is constructed from $M_{3\pi}$ (which should be near the mass of the a_1), the invariant masses of the two $\pi^+\pi^-$ combinations (one of which should be near the ρ mass), and the fraction of the event energy which is carried by the 3π system. The algorithm selects the correct three pions in 50% of all simulated $\tau \to 3\pi$ events.

We then construct a kinematic likelihood ratio, $\lambda_{3\pi}$, to suppress the dominant backgrounds: NC events, and CC events in which the lepton escapes particle identification (typically by not reaching the relevant detectors). The ratio $\lambda_{3\pi}$ contains the variables used to select the 3π system, as well as: functions of the transverse angles $\phi_{\tau_{\rm V} H}$ and ϕ_{mH}; the largest angle between one track in the 3π system and $\vec{p}^{\,\tau_{\rm V}}$; and the angle between $\vec{p}^{\,\tau_{\rm V}}$ and $\vec{p}^{\,H}$.

In order to reject CC interactions, one of the tracks must be selected as the most likely one to be the lepton. This selection is made using an auxiliary likelihood function constructed from the momentum components of the trial lepton and its isolation from the rest of the event; it has an efficiency of 89%. The isolation is quantified using a variable, R_T, which is computed by first defining the "transverse size" of a group of tracks as their average transverse-momentum-squared with respect to their total momentum. For every track i in the event, we calculate $R_T^{(i)}$, the ratio of the transverse size of all tracks except i to the transverse size of all tracks. For both CC and NC events, $R_T^{(i)}$ is typically of order of unity except when i is the CC lepton, in which case $R_T^{(i)}$ is smaller.

The ratio $\lambda_{3\pi}$ provides reduction in CC background, by biasing against events with the following CC characteristics: large p_T^ℓ for the lepton, small missing transverse momentum p_T^m, and trial lepton isolation. The magnitudes of p_T^ℓ and p_T^m are combined into the variable $\rho_\ell = p_T^\ell/(p_T^m + p_T^{\rm others} + p_T^\ell)$, where $p_T^{\rm others}$ is the p_T of the system of tracks not including ℓ.

Figure 5 contains histograms of the kinematic likelihood ratio $\ln\lambda_{3\pi}$ for (a) the $\tau^- \to \pi^-\pi^+\pi^-\nu_\tau$ search and (b) the control search for $\tau^+ \to \pi^+\pi^-\pi^+\bar{\nu}_\tau$. For each, we show the data superimposed on the MC prediction of the background. The signal region (to which we were blind) is at $\ln\lambda_{3\pi} > 8.8$ in (a). In order to remove residual ν_μ CC background, we apply a final lepton veto to the track (of either charge) having the highest p_T: the event is rejected if this track, if a muon, would have a low probability to reach the muon chambers. We also include in the lepton veto a cut against all events which have a primary track identified as an electron.

Following the final lepton veto, we observe 5 events in the 1995-96 data, compared to a background prediction of 6.5 ± 1.1, consistent with no oscillations. The corresponding analysis of the 1997 data is not yet complete.

Table 6 summarizes the effect of the main cuts on the data and various MC samples. The search for τ^+ shows good agreement between data and background expectations. In the τ^+ search, we still use the likelihood to reject the dominant *negative* leptons from CC events (just as in the τ^- search), and in fact the last survivors among MC events are ν_μ CC. Hence the τ^+ data-MC agreement is quite relevant to the τ^- search. Since there is no significant vari-

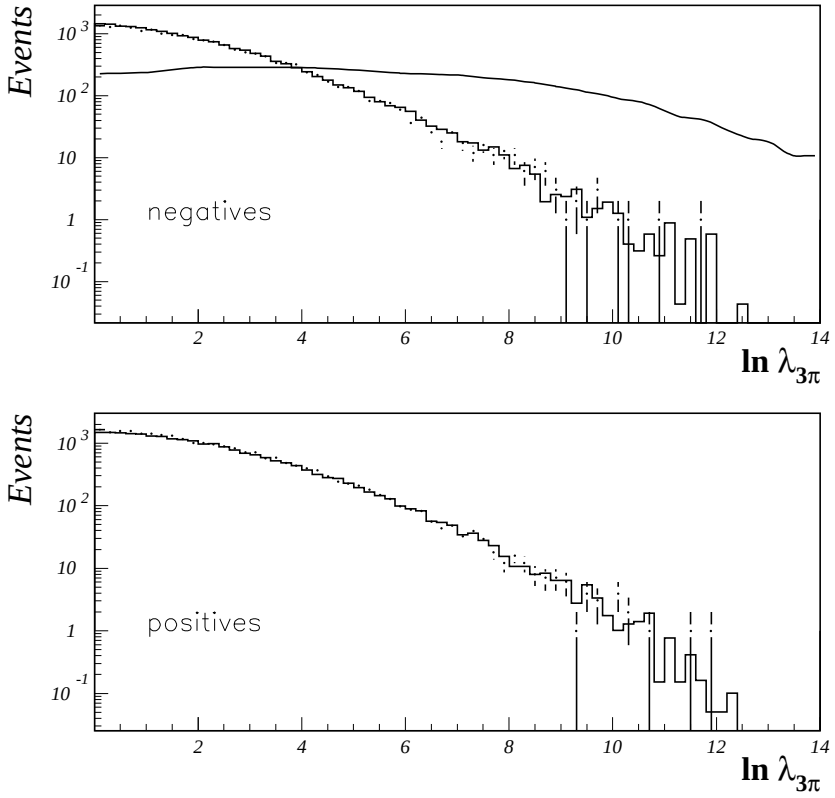

Fig. 5. Histogram of the kinematic likelihood ratio $\ln \lambda_{3\pi}$, prior to the final lepton veto, for (a) the $\tau^- \to \pi^-\pi^+\pi^-\nu_\tau$ search and (b) the control search for $\tau^+ \to \pi^+\pi^-\pi^+\bar{\nu}_\tau$, for MC (solid histograms) and data (with error bars). The additional curve in (a) is the smoothed signal MC. The histograms after the final lepton veto are just as consistent, but with less statistics.

Table 6
The effect of $\tau^- \to \pi^-\pi^+\pi^-\nu_\tau$ selection cuts on simulated signal events, on various background samples, and on the 1995-96 data. The ν_τ CC column shows efficiency with respect to the inclusive three-prong sample having a total branching ratio of 15.2%. The backgrounds are normalized to the event samples expected in the 1995-96 data. The effect of the cuts on the positive control sample is also shown.

Sample	ν_τ CC	ν_μ CC		$\bar{\nu}_\mu$ CC		ν_μ NC		ν_e CC		$\bar{\nu}_e$ CC		Data	
Charge	–	–	+	–	+	–	+	–	+	–	+	–	+
Preselection	0.573	24969	30029	220	234	45416	39031	1098	1828	146	126	66597	79001
$\ln \lambda_{3\pi} > 8.8$	0.038	7.0	18	0.8	0.2	4.9	2.5	4.1	12	1.1	0.7	14	30
Lepton veto	0.029	2.9	8.6	0.3	0.1	2.4	1.9	0.8	2.8	0.1	0.1	5	14

ation of the signal-to-background ratio within the box, no sub-boxes are used in this case.

The results for all hadronic decays of the τ^- are summarized in Table 7.

Table 7
Events remaining in the signal region from the $\tau^- \to$ hadrons $+ \nu_\tau$ searches (total background and data). $N_\tau^{\max}$ is described in Sec. 9; it is the number of τ^- events expected if the $\nu_\mu \to \nu_\tau$ oscillation probability were unity.

Decay Channel	Sub-box #	Total background	Data	$N_\tau^{\max}$
$\tau \to h(n\pi^0)$	I	2.7 ± 0.9	3	564
	II	0.5 ± 0.5	2	200
	III	1.8 ± 0.7	0	963
$\tau \to \rho$	–	$5.0^{+1.7}_{-0.9}$	5	1891
$\tau \to 3\pi(\pi^0)$	–	6.5 ± 1.1	5	1180

Table 8
Summary of backgrounds and efficiencies for all analyses described here (DIS) and for the analysis of low-multiplicity (LM) events reported in [1]. The column τ^- summarizes the observed number of τ^- candidate events (Obs.) and the corresponding predicted background (Est. Bkgnd) for each channel. The column τ^+ contains the equivalent numbers for "wrong sign" candidates. The corresponding τ^- selection efficiencies (ϵ) and τ branching ratios (Br) are also listed. Finally, the maximum number of expected signal events ($N_\tau^{\max}$), as computed from Eq. (1), is indicated for each channel.

	τ^-		τ^+				
Analysis	Obs.	Est. Bkgnd	Obs.	Est. Bkgnd	$\epsilon(\%)$	$Br(\%)$	$N_\tau^{\max}$
$\tau \to e$ DIS	5	$6.3^{+1.6}_{-1.0}$	7	7.4 ± 3.1	3.5	17.8	2818
$\tau \to h(n\pi^0)$ DIS	5	5.0 ± 1.2	14	9.9 ± 2.3	0.78	49.8	1727
$\tau \to \rho$ DIS	5	$5.0^{+1.7}_{-0.9}$	13	$10.2^{+1.4}_{-1.1}$	1.6	25.3	1891
$\tau \to 3\pi(\pi^0)$ DIS	5	6.5 ± 1.1	14	13.5 ± 1.4	2.9	15.2	1180
$\tau \to e$ LM	0	$0.5^{+0.6}_{-0.2}$	1	1.1 ± 0.7	3.4	17.8	218
$\tau \to \pi(\pi^0)$ LM	1	$0.1^{+0.3}_{-0.1}$	6	8.8 ± 3.5	1.5	37.3	198
$\tau \to 3\pi(\pi^0)$ LM	0	$0.4^{+0.6}_{-0.4}$	14	11 ± 4	2.0	15.2	108

9 The limit for $\nu_\mu \to \nu_\tau$ oscillations

We express the result of the measurements described above as a frequentist confidence interval [13] by optimally combining the measurements for each channel, taking into account the number of observed signal events, the expected background and its uncertainty, and the number of expected signal events if the oscillation probability were unity. This last quantity is given by

$$N_\tau^{\max} = N_\mu^{\rm obs} \times (\sigma_\tau/\sigma_\mu) \times Br \times (\epsilon_\tau/\epsilon_\mu), \qquad (1)$$

where:

- $N_\mu^{\rm obs}$ is the observed number of ν_μ CC interactions corresponding to the conditions of the analysis in question.
- ϵ_τ and ϵ_μ are the detection efficiencies for τ signal events and ν_μ CC normalization events. The cuts used to select $N_\mu^{\rm obs}$, and hence also ϵ_μ, vary from channel to channel in order to reduce systematic errors in the ratio $\epsilon_\tau/\epsilon_\mu$ for that channel.
- (σ_τ/σ_μ) is the suppression factor of the ν_τ cross section due to the difference between the τ and μ masses. It is calculated to be 0.48 for the analyses described in this paper.
- Br is the branching ratio for the τ decay channel in question.

These quantities are summarized in Table 8, which includes the published results from the analysis of low-multiplicity events in the 1995 data [1], selected by requiring $p^H < 1.5$ GeV/c.

The systematic uncertainty on $N_\tau^{\rm max}$ is estimated to be 10%, resulting mostly from the uncertainty on the efficiency calculations [15].

To construct the confidence region, we wish to exploit optimally the fact that results from different τ decay modes and sub-boxes have different ratios of $N_\tau^{\rm max}$ to background. We therefore treat each analysis and each sub-box as a "bin" in the spirit of Eq. (5.6) of Ref. [13]. However, the mean expected backgrounds have uncertainties resulting from the limited statistics of the MC and DS samples. To account for these, we replace the likelihood ratio in Eq. (5.4) of Ref. [13] with a generalized approximate [2] form [16]

$$R = \frac{P(x|\mu+\hat{\hat{\beta}})P(b|\hat{\hat{\beta}})}{P(x|\mu_{\rm best}+\hat{\beta})P(b|\hat{\beta})} \qquad (2)$$

where:

- $P(y|z)$ denotes the probability to measure y given the true value z,
- μ and β are the unknown true values of the signal and background parameters,
- x and b are measurements of $\mu+\beta$ and β respectively (in our case, b is determined from a MC and DS "experiment" with finite statistics),
- $\mu_{\rm best}$ and $\hat{\beta}$ are the values of μ and β which maximize the denominator, and
- $\hat{\hat{\beta}}$ is chosen to maximize the numerator depending on μ.

Tables 2, 7 and 8 do not include an additional systematic error on the background prediction (primarily due to residual uncertainties in the DS correc-

[2] We checked that this approximation still provides frequentist coverage in our case.

tion), which we estimate to be 20%. Since the different τ decay modes are dominated by different background sources, this error is only mildly correlated between modes. We therefore combine it in quadrature with the statistical errors. Its effect on the combined limit is negligible.

The resulting 90% C.L. upper limit on the two-generation oscillation probability is

$$P_{\rm osc}(\nu_\mu \to \nu_\tau) < 0.6 \times 10^{-3}, \tag{3}$$

which corresponds to $\sin^2 2\theta_{\mu\tau} < 1.2 \times 10^{-3}$ for large Δm^2 and to the exclusion region in the $\Delta m^2 - \sin^2 2\theta$ plane shown in Fig. 6. This is an improvement by a factor of 3.5 on our previous result [1].

The sensitivity of the experiment (defined in Sec. 4.2) is $P_{\rm osc} = 1.0 \times 10^{-3}$; this is higher than the quoted confidence limit, since the number of observed events is fewer than the estimated background. In the absence of signal events, the probability to obtain an upper limit of 0.6×10^{-3} or lower is 28%. The sensitivity would have been worse by about 30% in the case of a single bin analysis (summing all channels) and is made worse by about 10% by the presence of the background uncertainty.

10 Conclusion

Using events with DIS topology from the 1995, 1996, and 1997 NOMAD data sets, combined with the previously reported analyses of the low-multiplicity 1995 events, we have excluded a region of oscillation parameters which limits (at 90% C.L.) $\sin^2 2\theta_{\mu\tau}$ at high Δm^2 to values less than 1.2×10^{-3}, and which limits Δm^2 to values less than $\Delta m^2 < 1.2$ eV$^2/c^4$ at $\sin^2 2\theta_{\mu\tau} = 1$. We expect to improve the sensitivity by adding more data, primarily low-multiplicity events from 1996-97 and data of all topologies from the recently completed 1998 run (the final run for NOMAD).

Acknowledgement

We thank the management and staff of CERN and of all participating institutes for their vigorous support of the experiment. Particular thanks are due to the CERN accelerator and beam-line staff for the magnificent performance of the neutrino beam. The following funding agencies have contributed to this experiment: Australian Research Council (ARC) and Department of Industry, Science, and Resources (DISR), Australia; Institut National de Physique

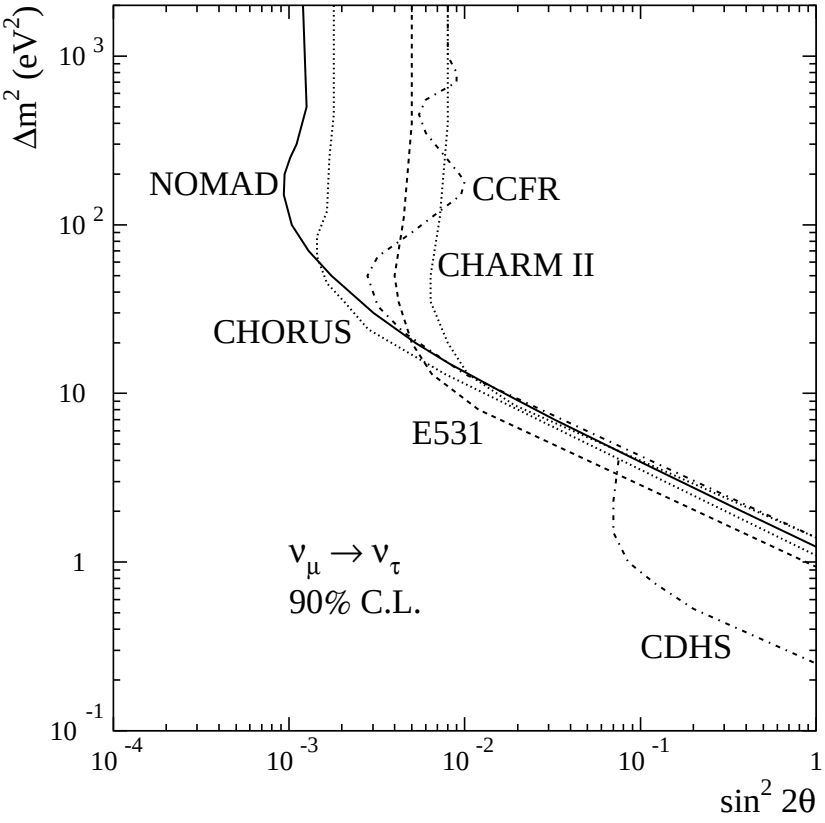

Fig. 6. The $\Delta m^2 - \sin^2 2\theta$ plane. The region excluded by NOMAD at 90% C.L. (solid line) is shown together with limits published by other experiments [17–19].

Nucléaire et Physique des Particules (IN2P3), Commissariat à l'Energie Atomique (CEA), Ministère de l'Education Nationale, de l'Enseignement Supérieur et de la Recherche, France; Bundesministerium für Bildung und Forschung (BMBF, contract 05 6DO52), Germany; Istituto Nazionale di Fisica Nucleare (INFN), Italy; Russian Foundation for Basic Research, Institute for Nuclear Research of the Russian Academy of Sciences, Russia; Fonds National Suisse de la Recherche Scientifique, Switzerland; Department of Energy, National Science Foundation (grant PHY-9526278), the Sloan and the Cottrell Foundations, USA. F.J.P. Soler is supported by a TMR Fellowship from the European Commission.

We also thank our secretarial staff, Jane Barney, Marie-Anne Huber, Rachel Phillips, and Mabel Richtering, and the following people who have worked with the collaboration on the preparation and the data collection stages of NOMAD: M. Anfreville, M. Authier, A. Beer, V. Bonaiti, A. Castera, O. Cloué, C. Détraz, L. Dumps, C. Engster, G. Gallay, W. Huta, E. Lessmann, J. Mulon, J.P. Passérieux, P. Petitpas, J. Poinsignon, M. Serrano, C. Sobczynski, S. Soulié, L. Visentin, P. Wicht. We dedicate this article to the memory of our

collaborators A. Cavestro and G. Fumagalli.

References

[1] NOMAD Collaboration, J. Altegoer, et al., Phys. Lett. B 431 (1998) 219.

[2] Preliminary results from this analysis are reported by D. Autiero (NOMAD Collaboration), Proceedings of the XXIX International Conference on High Energy Physics (ICHEP '98), Vancouver, B.C., Canada, 23-29 July 1998, to be published.

[3] S.N. Gninenko, Nucl. Instr. and Meth. A 409 (1998) 583; D. Autiero et al., Nucl. Instr. and Meth. A 411 (1998) 285; D. Autiero et al., CERN-EP/98-126, accepted for publication in Nucl. Instr. and Meth. A.

[4] NOMAD Collaboration, J. Altegoer et al., Nucl. Instr. and Meth. A 404 (1998) 96.

[5] G. Bassompierre et al., Nucl. Instr. and Meth. A 403 (1998) 363; G. Bassompierre et al., Nucl. Instr. and Meth. A 411 (1998) 63.

[6] D. Autiero et al., Nucl. Instr. and Meth. A 372 (1996) 556; D. Autiero et al., Nucl. Instr. and Meth. A 373 (1996) 358; D. Autiero et al., Nucl. Instr. and Meth. A 387 (1997) 352.

[7] J. Altegoer et al., CERN-EP/98-202, accepted for publication in Nucl. Instr. and Meth. A.

[8] G. Collazuol et al., presented at NOW98 Workshop, Amsterdam, 7-9 September 1998, CERN Preprint OPEN-98-032. The prompt ν_τ component is negligible; see M.C. Gonzales-Garcia, J.J. Gomez-Cadenas, Phys. Rev. D 55 (1997) 1297; B. Van de Vyver, Nucl. Instr. and Meth. A 385 (1997) 91.

[9] G. Ingelman, LEPTO 6.1, in Proc. of Physics at HERA, Edited by W. Buchmueller, G. Ingelman, DESY, Hamburg (1992) 1366;

[10] T. Sjöstrand, Computer Phys. Commun. 39 (1986) 347; T. Sjöstrand and M. Bengtsson, Computer Phys. Commun. 43 (1987) 367; T. Sjöstrand, Computer Phys. Commun. 82 (1994) 74.

[11] A. Bodek and J. Ritchie, Phys. Rev. D 23 (1981) 1070.

[12] GEANT, CERN Program Library Long Writeup W5013.

[13] G.J. Feldman, R.D. Cousins, Phys. Rev. D 57 (1998) 3873.

[14] C. Albright, R. Shrock, Phys. Lett. B 84 (1979) 123.

[15] The effect of this systematic uncertainty on the limit calculation is negligible if it is treated in the manner of R.D. Cousins, V.L. Highland, Nucl. Instr. and Meth. A 320 (1992) 331.

[16] A. Stuart, J.K. Ord, *Kendall's Advanced Theory of Statistics,* vol. 2, *Classical Inference and Relationship* 5th Ed. (Oxford Univ. Press, New York, 1991), p. 861, Eq. 23.4.

[17] E531 Collaboration, N. Ushida et al., Phys. Rev. Lett. 57 (1986) 2897.

[18] CHORUS Collaboration, E. Eskut et al., Phys. Lett. B 424 (1998) 202; Phys. Lett B 434 (1998) 205.

[19] CHARM-II Collaboration, M. Gruwe et al., Phys. Lett. B 309 (1993) 463; CCFR Collaboration, K.S. McFarland et al., Phys. Rev. Lett. 75 (1995) 3993; CDHS Collaboration, F. Dydak et al., Phys. Lett. B 134 (1984) 281.